Journal of Biological Physics **29:** 247–256, 2003.

T-ray Imaging and Tomography

S. WANG[1], B. FERGUSON[1,2], D. ABBOTT[2] and X.-C. ZHANG[1]*
[1] *Center for Subsurface Sensing and Imaging Systems, Rensselaer Polytechnic Institute, Troy, NY 12180-3590 USA*
[2] *Centre for Biomedical Engineering and the Department of Electrical & Electronic Engineering, The University of Adelaide, SA, 5005, Australia*
(*Author for correspondence, e-mail: zhangxc@rpi.edu)

Abstract. We demonstrate two algorithms used for reconstructing the target's structure based on the diffracted pulses and additionally show that a three-dimensional target can be reconstructed using the broadband pulses and a Fresnel lens by virtue of its frequency dependent focal length. One advantage of T-ray imaging is the ability to measure the far-infrared spectral response of the target. To highlight the importance of this spectral information, we demonstrate T-ray classification imaging with different biological samples using a simple classification algorithm and two dimensional T-ray spectroscopic images.

Key words: Imaging, tomography, T-rays

Introduction

Terahertz (THz) wave occupies a large portion of the electromagnetic spectrum between infrared and microwave band ranging from 0.1 to 20 THz, has wide potential application in material science, astronomy and biomedical fields. For over a decade, ultrashort THz pulses have been investigated for applications including measuring the optical properties of materials in the sub-millimeter wavelength regime, tissue burn diagnostics and DNA analysis [1, 2]. THz time domain spectroscopy (THz TDS) [3] is one of the most interesting technologies. THz TDS is coherent in that it provides the measurement of THz electric field $ETHz(t)$ rather than of the intensity $|ETHz(t)|^2$. As a result, the phase information is preserved, and one may determine the sample's complex dielectric function without resorting to Kramers-Kronig relationship.

The photon energies of THz radiation is in the range 0.4 to 80 meV, which corresponds to the range of energies associated with changes between molecular energy level [4]. Using transition frequency information and the complex refractive response function, it is possible to identify the chemical components of samples. Mittleman's group demonstrated real time gas mixture analysis using THz TDS [1]. Brucherseifer et al have undertaken the time-resolved THz transmission analysis

of polynucleotides, which confirms that the complex refractive index is strongly dependent on the hybridization state of DNA molecules [5].

One of the main applications of THz TDS is imaging. In imaging applications, it would be valuable not only to generate the structure image of the sample but also perform spectroscopic analysis and identification. THz TDS imaging allows local THz spectra to be determined at every image pixel. Various THz image techniques have been demonstrated in past decade [6–8], for applications as diverse as moisture analysis, package inspection, biomedical diagnosis, and gas sensing.

Three dimensional (3D) T-ray imaging has been an important recent focus. Reflection mode THz tomographic imaging has been demonstrated [9], however, the reconstruction algorithms are based on the assumption of negligible dispersion and therefore the spectra information is lost. Recently T-ray computed tomography based on the assumption of straight-line propagation of THz radiation according to the Radon transform [10, 11]. Here we present several THz 3D tomographic imaging modalities based on a wave equation propagation model incorporating diffraction. These methods potentially allow more general targets to be imaged. Section 1 presents the T-ray diffraction tomography system and describes two methods of image reconstruction. Section 2 describes an additional tomographic imaging method which utilizes a Fresnel lens to image each tomographic slice simultaneously by considering the image formed by each frequency component of the broadband THz pulses. We then illustrate the power of T-ray spectroscopic imaging by considering the problem of the identification of unknown powders within envelopes. A classification system for 2D T-ray spectroscopic images is presented in Section 3. Finally Section 4 discusses the implications and future directions of this work.

1. THz Diffraction Tomography

Neglecting polarization THz waves satisfy the scalar Helmholtz wave equation

$$\nabla^2 u(r) + k(r)^2 u(r) = 0 \tag{1}$$

where $u(r)$ is the THz distribution function and $k(r)$ is the wave number of the THz field. For simple samples consisting of well separated layers in a homogenous background media we can develop a simple tomographic reconstruction algorithm, which avoids the need to invert the Helmholtz equation. THz-TDS measures the THz time domain waveform, provided the THz pulse is short enough, it is possible to truncate the scattered waves to obtain the local spectra that resulted from each layer of the target. By Fourier transforming the truncated time domain pulses we can perform a tomographic reconstruction using a back propagation algorithm at all available THz frequencies. In the case of a homogenous background the wave number is a constant and, the scattered wave can be predicted by the Rayleigh-Sommerfeld diffraction formula [12],

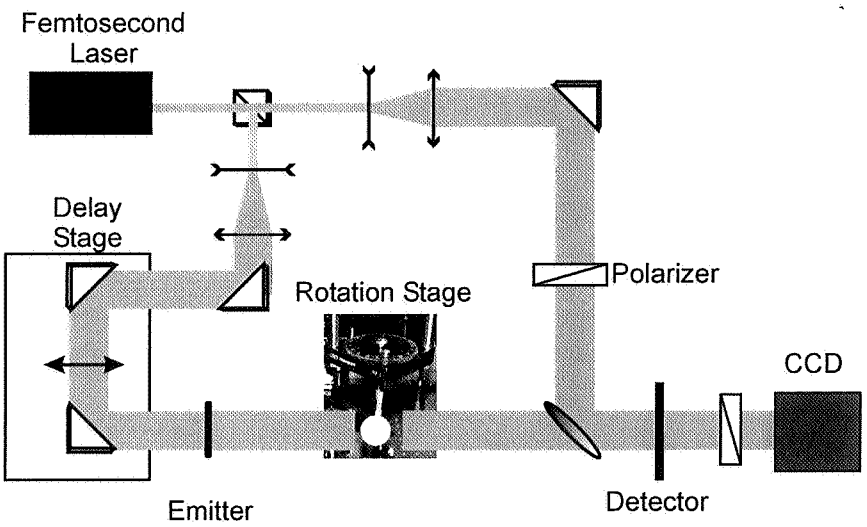

Figure 1. T-ray DT schematic setup. Lenses were used to expand the pump and probe beams to a diameter of 2.5 cm. THz pulses were generated using a wide aperture photoconductive antenna and detected using 2D electro-optic sampling in a 4 mm thick <110> ZnTe detector crystal.

$$u(P_0) = \frac{1}{j\lambda}\int\int_A u(P_1)\frac{\exp(jkr_{01})}{r_{01}}\cos(\bar{n}, r_{01})ds \tag{2}$$

where r_{01} is the distance between the measurement point and a point in the target, $\bar{n}$ is the measurement surface normal and A is a measurement surface. For any solution *u(k; r)* of Eq. (1), *u(-k; r)* is also a solution. Based on the measured scattered wave, we can reconstruct the scattering centers by reversing the wave propagation direction and using Eq. (2) to predict the scattering center distribution. This method is similar to the method described in Ref. [13], which performed backpropagation of the time domain Rayleigh equation to reconstruct a 2D aperture image.

Figure 1 shows the imaging system used to study the THz diffraction. THz pulses were generated using a regeneratively amplified Ti:sapphire laser (Spectra Physics Hurricane) with an average output power of 700 mW, center wavelength of 800 nm, a pulse duration of 130 fs and a repetition rate of 1 kHz, incident on a 14 mm wide aperture photoconductive antenna with a bias of 2000 V. The pump and probe beams were expended to 25 mm (1/e) and resulted in the generation of approximately plane wave THz radiation with a beam diameter of 25 mm. The 2D THz formed on the EO crystal (4 mm thick <110> ZnTe) modulated the probe beam pulse via the EO effect. The image carried by the probe beam was focused onto a CCD camera by a lens.

Figure 2 shows the schematic of a simple targets' arrangement and the reconstructed image of the target resulting from equation (2). Here we used the windowed Fourier transformation to obtain local spectra, and applied the image

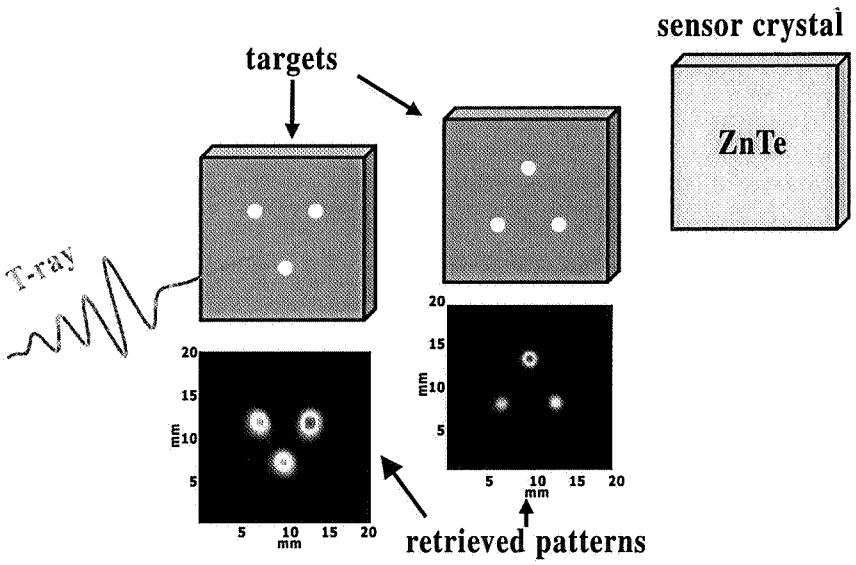

Figure 2. The schematic target arrangement and reconstructed image of the target according to equation (2), The targets are Polyethylene plastics sheets with holes patterns. The distance between 2 samples are 4.5 cm. The reconstructed image shows the correct spatial relationship between these holes.

reconstruction using each window. The hole pattern on the 2 samples was correctly reconstructed.

In more general case, the wave number is a spatial function. In this case we utilize classical diffraction tomography methods to solve a linearized form of the Helmholtz equation. We rewrite the wave equation

$$(\nabla^2 + k_0^2)u_s(r) = -u(r)o(r) \tag{3}$$

where the field $u(r)$ is the sum of the incident, $u_0(r)$ and scattered $u_s(r)$ components, $o(r)$ is the target function of interest and k_0 is the wave number of the background medium. We deal with the reconstruction at a single frequency, which is achieved by Fourier transforming the received pulses. A solution to this equation can be obtained in terms of the Green's function,

$$u_s(r) = \int G(r - r')o(r)u(r')dr' \tag{4}$$

This equation cannot be solved directly. In order to resolve it, we need to use the Born and Rytov approximations. T-ray tomographic imaging technology is based on these two approximations [14]. Using this reconstruction algorithm we measure the diffracted field on the CCD for a number of projection angles. This is accomplished by rotating the sample. The Fourier Diffraction theorem and interpolation in the spatial frequency domain are then used to reconstruct the spatial object function. In T-ray experiments we found that Rytov approximation provided more

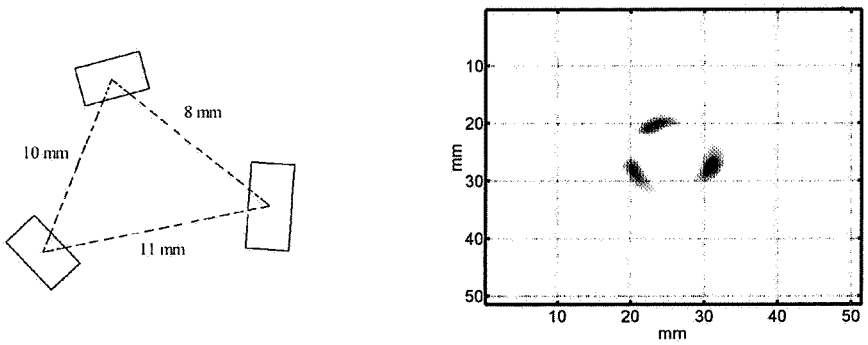

Figure 3. (a) The geometry of polyethylene rectangular cylinders, which dimensions of 2.0 mm by 1.5 mm, 3.5 mm by 1.5 mm and 2.5 mm by 1.5 mm. (clockwise from top). (b) Reconstructed cross-section of the polyethylene cylinders.

accurate solution. We used a sample to test this system. The sample is consisted of 3 polyethylene rectangular cylinders; its cross section is illustrated schematically in Figure 3a. The reconstruction was performed using a frequency of 0.2 THz, which provided the maximum signal to noise ratio (SNR) for our antenna source. The reconstructed cross section reflected the correct spatial relationship between the 3 cylinders.

The present methods are only applicable to weakly scattering objects. In the future non-linear iterative techniques will enable more general targets to be reconstructed.

2. Fresnel Lens Tomography

The focal length of a Fresnel lens is linearly proportional to frequency. This unique property allows tomographic imaging of a target using multiple frequencies. Using a Fresnel lens at different frequencies of the imaging beam, we are able to image the objects at various positions along the beam propagation path onto the same imaging plane. This procedure enables the reconstruction of an object's tomographic contrast image by assembling the frequency-dependent images. A binary lens is a Fresnel zone plate with phase or amplitude modulated patterns, formed by a series of concentric ring structures. The main focal length is defined as,

$$f_\nu = \frac{r_p^2}{2\lambda} = \frac{r_p^2}{2c}\nu \propto \nu \tag{5}$$

where r_p^2 is the Fresnel zone period with a dimension of area, λ is the wavelength, c is the speed of light, and ν is the frequency. The focal length f_ν is linearly proportional to frequency ν. For a single-lens imaging system, under the paraxial ray approximation, the relationship between object distance z, image distance z' and the focal length f_ν is governed by the imaging equation,

$$\frac{1}{z}+\frac{1}{z'}=\frac{1}{f_\nu} \tag{6}$$

If the image plane position is fixed, and therefore z is fixed, for a wave with frequency ν, due to the frequency dependent focal length f_ν, the object distance z is also frequency dependent. Combining Eqs. 5 and 6, yields,

$$z=\frac{f_\nu z'}{z'-f_\nu}=\frac{r_p^2 z'\nu}{2cz'-r_p^2\nu} \tag{7}$$

At each frequency ν, there is a corresponding value of z, and a target at this position z can be well imaged onto the position z' at the imaging plane. In order to keep the imaging distance $z > 0$, it requires $z' > r_p^2\nu/2c$. The experimental setup of the imaging system with a CCD camera was similar to the one used for the characterization of a THz wave reported elsewhere. [15] A 30-mm diameter silicon binary lens with a focal length of 2.5 cm at 1 THz was used as the THz wave Fresnel lens. The measured two-dimensional THz field distribution at each frequency formed the image of THz field transmission of a target at each corresponding position along the z-axis. Figure 4 schematically illustrates the tomographic imaging arrangement. Three plastic sheets with different patterns were placed along the THz beam path, and their distances to the lens, corresponding to z in Eqn. 7 were 3 cm, 7 cm and 14 cm, respectively. Inverted images of patterns on the sensor plane at distance $z' = 6$ cm were measured at frequencies of 0.74 THz, 1.24 THz, and 1.57 THz, respectively. At each frequency, the Fresnel lens imaged a different plane section of a target object corresponding to a certain depth while images from other depths remained blurred. Each point in the different object planes along the z-axis was mapped onto a corresponding point on the z' plane (sensor plane) with the magnification factor z'/z at their corresponding frequencies. The ratio of the measured image size to the actual size of the pattern agreed well with the calculated magnification factor.

3. T-ray 2D Classification Imaging

The ultimate goal in all terahertz systems is to extract information of the sample under test. Here we desire to detect and differentiate between different samples based on their terahertz response. Classification involves producing meaningful material distribution maps via identification of individual pixels or groups of pixels with similar spectral responses (spectral signatures). These pixels or groups represent different materials or classes. The actual data associated with each pixel are analyzed mathematically using computer driven algorithms.

We have demonstrated a simple classification system using the Mahalanobis [16] distance as the discriminant function. This is one of a class of minimum distance classifiers. It assumes that the data for each class are normally distributed, thus the samples drawn from each class will form a cluster in N dimensions, with a center given by the mean vector, μ, and shape dependent on the covariance matrix, Σ. These parameters can be estimated,

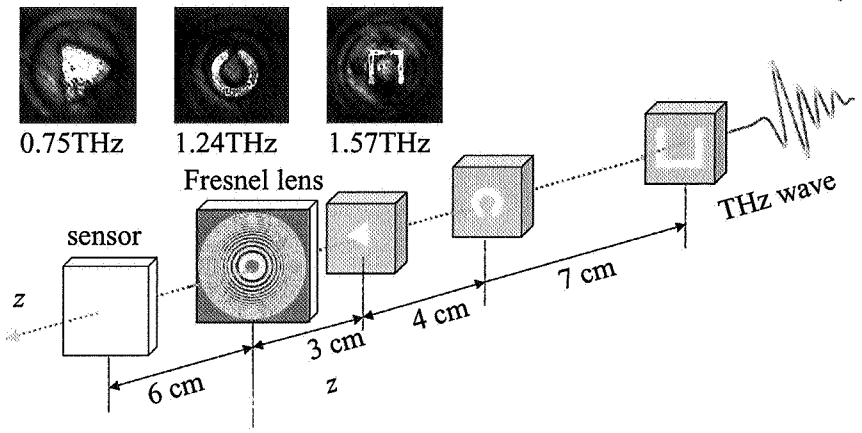

Figure 4. Schematic illustration of the tomographic imaging with a Fresnel lens. Targets at various locations along the beam propagation path are uniquely imaged on the same imaging sensor plane with different frequencies of the imaging beam. Three plastic sheets were cut with different patterns placed 3 cm, 7 cm, and 14 cm away from the Fresnel lens. The multiple patterns are imaged on the sensor at a distance of 6 cm from the Fresnel lens, with inverted tomography images of the patterns at the frequencies of 0.75 THz, 1.24 THz and 1.57 THz, respectively. The measured image size is determined by the frequency dependent magnification factor, which is defined as z'/z.

$$\mu = E[X],$$
$$\Sigma = E[(X-\mu)(X-\mu)^T \tag{8}$$

The Mahalanobis distance calculates the distance of a given point from the mean value for a given class normalized by the variance of the training vectors in that direction. For a given class, k, the distance is defined as,

$$d_k(X) = (X-\mu_k)^T \Sigma^{-1} (X-\mu_k)^T \tag{9}$$

Classification is performed by selecting the class that has the minimum Mahalanobis distance.

A number of samples were imaged using a 2D THz imaging system. The system utilized a chirped probe pulse to allow the THz temporal profile to be measured simultaneously and raster scanned the target to obtain the THz response at each pixel. This system has been described in detail previously [17].

The samples imaged were a powder pattern and an envelope containing *Bacillus thuringiensis* (BT) spores. Figure 5 shows an optical image, THz image, classified image and waveforms of the powders respectively. Four different powdered samples: flour, salt, baking soda and seasoning (800 milligrams of each) were placed inside a paper envelope and imaged with THz system. The four powders have very similar THz responses (Figure 5d), however, the minor differences in THz transmission waveform can be discriminated using the classification algorithm, and the classification result is shown in Figure 5c, which clearly shows that the pattern consisted of different classes.

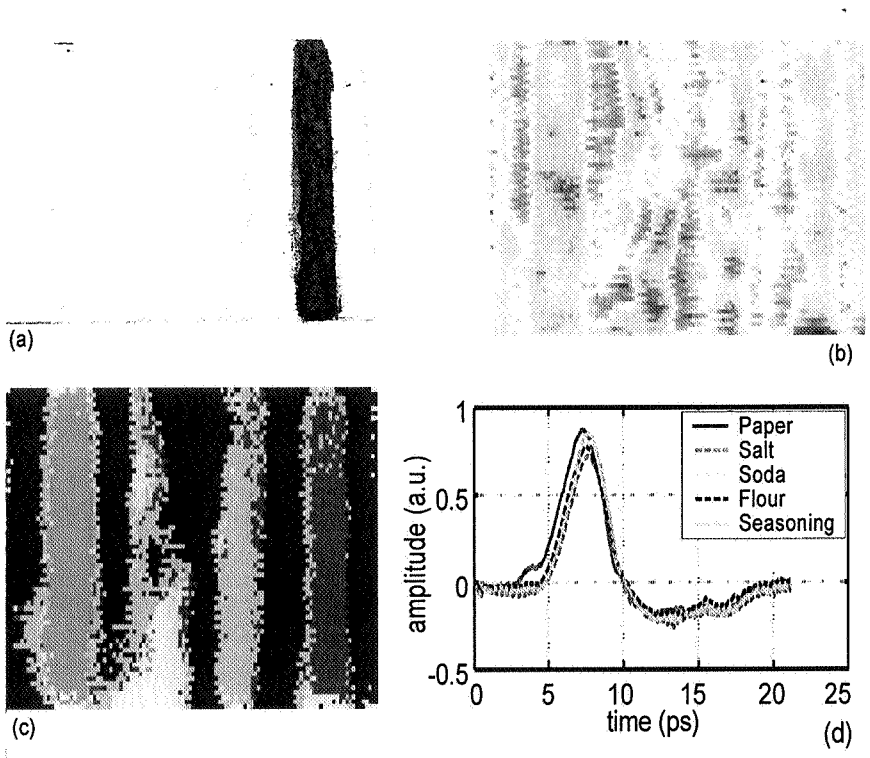

Figure 5. (a) The photograph of the pattern formed by four different powders, from left to right: flour, salt, baking soda and seasoning (800 milligrams of each). (b) The THz image of the powder sample that placed inside a paper envelope. (c) The classified THz image using the classification algorithm, this image shows that the pattern consisted of different classes labeled with different colors.

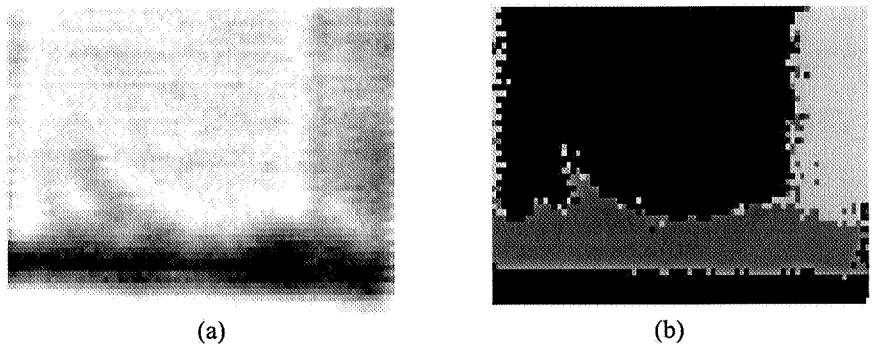

Figure 6. (a) The THz image of envelop containing 500 milligrams of *B. thuringiensis* spore, the image was taken at 0.3 THz. (b) The THz classification result, the *B. thuringiensis* spore was located at the middle bottom.

To assess the applicability of THz imaging to Anthrax detection we considered samples of BT bacteria. We used BT as a safe alternative to *Bacillus anthracis* (anthrax). BT can be used to closely simulate anthrax due to the fact that the BT genome is identical to that of anthrax, apart from a short DNA sequence that codes for the toxin – for this reason they are regarded as even being the same species [18]. While the anthrax toxin is fatal to humans, the BT toxin is only fatal to insects. Approximately 500 milligrams of *B. thuringiensis* spore flakes were placed inside an envelope shown as Figure 6a, and then imaged using the THz system. The THz classification result is shown in Figure 6b.

4. Conclusion

T-ray diffraction tomography is very attractive due to its ability to extract the frequency dependent refractive index at each pixel of a 3D image. It can be performed relatively quickly by aid of 2D THz imaging, and the diffracted field is explicitly used in the reconstruction allowing a wide class of targets to be reconstructed. Future work in T-ray DT systems will focus on improving the signal to noise ratio and the development of accurate and robust reconstruction algorithms. A Fresnel lens allows tomographic images to be obtained without requiring rotation of the target; it has the potential to acquire 3D images of targets quickly. However, this method does not provide spectroscopic information.

The THz spectrum is a rich source of material information and allows the identification of material species such as bacterial spores hidden inside optically opaque material. The preliminary experiment result shows that T-ray classification imaging can be used to obtain identification images. The computational complexity of the algorithms is a vital concern as systems head towards real-time data acquisition. This could be improved further by optimizing the software implementation.

Applications of these techniques may include 3-dimensional biological imaging and anthrax and TNT detection for mail, package and luggage screening.

This work was supported in part by the Center for Subsurface Sensing and Imaging Systems, under the Engineering Research Centers Program of the National Science Foundation (award number EEC-9986821). We are grateful to Mr. Edward Walsby of the University of Canterbury, New Zealand for providing the silicon binary lens. Bradley Ferguson thanks the Australian-American Fulbright Commission.

References

1. Mittleman, D.M., Jacobsen, R.H., Baraniuk, R.G. and Nuss, M.C.: Gas Sensing using Terahertz Time-Domain Spectroscopy, *Appl. Phys. B* **67** (1998), 379–390.
2. Nagel, M., Bolivar, P.H., Brucherseifer, M. and Kurz, H.: Integrated THz Technology for Label-free Genetic Diagnostics, *Appl. Phys. Lett.* **80** (2002), 154–157.

3. Dahl, C., Genzel, L., Goy, P., Gruner, G., Kotthaus, J.P., Kozlov, G., Nuss, M.C., Orenstein, J. and Volkov, A.: Terahertz Time-domain Spectroscopy, In: *Millimeter and Submillimeter Wave Spectroscopy of Solids,* Springer-Verlag, Berlin, Germany, 1998, pp. 7–50.
4. Svanberg, S.: *Atomic Molecular Spectroscopy*, 2nd edn., Springer, Berlin, 1992.
5. Brucherseifer, M., Nagel, M., Bolivar, P.H., Bosserhoff, A., Buettner, R. and Kurz, H.: Label-free Probing of the Binding State of DNA by Time-domain Terahertz Sensing, *Appl. Phys. Lett.* **77** (2000), 4049–4051.
6. Hu, B.B. and Nuss, M.C.: Imaging with Terahertz waves, *Opt. Lett.* **20** (1995), 1716–1719.
7. Hunsche, S., Koch, M., Brener, I. and Nuss, M.C., Terahertz near Field Imaging, *Opt. Commun.* **150** (1998), 22–26.
8. Jiang, Z. and Zhang, X.-C.: Single-Shot Spatiotemporal Terahertz Field Imaging, *Opt. Lett.* **23** (1998), 1114–1117.
9. Mittleman, D.M., Hunsche, S., Bovin, L. and Nuss, M.C.: T-ray Tomography, *Opt. Lett.* **22** (1997), 904–907.
10. Ferguson, B., Wang, S., Gray, D., Abbott, D. and Zhang, X.-C.: T-ray Computed Tomography, *Opt. Lett.* **27** (2002), 1312–1315.
11. Ferguson, B., Wang, S., Gray, D., Abbott, D. and Zhang, X.-C.: Towards Functional 3D THz Imaging, *Phys. Med. Biol.* **47** (2002), 4735–4742.
12. Goodman, J.W.: *Introduction to Fourier Optics,* McGraw-Hill, New York, 1996.
13. Ruffin, A.B., Decker, J., Sanchez-Palencia, L., Hors, L.L., Whitaker, J.F., Norris, T.B. and Rudd, J.V.: Time Reversal and Object Reconstruction with Single-Cycle Pulses *Opt. Lett* **26** (2001), 681–684.
14. Kak, A.C. and Slaney: *Principles of Computerized Tomographic Imaging*, Society of Industrial and Applied Mathematics, 2001.
15. Wang, S., Yuan, T., Walsby, E.D., Blaikie, R.J., Durbin, S.M., Cumming, D.R.S., Xu, J. and Zhang, X.-C.: Characterization of T-ray Binary Lenses, *Opt. Lett.* **27** (2002), 1183–1186.
16. Schuermann, J.: *Pattern Classification – A Unified View of Statistical and Neural Approaches*, John Wiley & Sons, Inc., New York, 1996.
17. Ferguson, B., Wang, S., Gray, D., Abbott, D. and Zhang, X.-C.: T-ray Tomographic Imaging, *Microelec. J.* (2002), in press.
18. Helgason, E., Okstad, O.A., Caugant, D.A., Johansen, H.A., Fouet, A., Mock, M., Hegna, I. and Kolsto, A.-B.: *Bacillus anthracis, Bacillus cereus*, and *Bacillus thuringiensis* – One Species on the Basis of Genetic Evidence, *Appl. Env. Microbiol.* **66** (2000), 2627–2630.